Prolate-Spherical Shape Coexistence at $N = 28$ in ^{44}S

C. Force,[1] S. Grévy,[1] L. Gaudefroy,[2] O. Sorlin,[1] L. Cáceres,[1] F. Rotaru,[3] J. Mrazek,[4] N. L. Achouri,[5] J. C. Angélique,[5] F. Azaiez,[6] B. Bastin,[5] R. Borcea,[3] A. Buta,[3] J. M. Daugas,[2] Z. Dlouhy,[4] Zs. Dombrádi,[7] F. De Oliveira,[1] F. Negoita,[3] Y. Penionzhkevich,[8] M. G. Saint-Laurent,[1] D. Sohler,[7] M. Stanoiu,[3] I. Stefan,[1] C. Stodel,[1] and F. Nowacki[9]

[1]*Grand Accélérateur National d'Ions Lours (GANIL), CEA/DSM-CNRS/IN2P3, Caen, France*
[2]*CEA,DAM,DIF, F-91297 Arpajon, France*
[3]*Institute of Atomic Physics, IFIN-HH, Bucharest-Magurele, P.O. Box MG6, Romania*
[4]*Nuclear Physics Institute, AS CR, CZ-25068 Rez, Czech Republic*
[5]*LPC Caen, ENSICAEN, Université de Caen, CNRS/IN2P3, Caen, France*
[6]*IPNO, Université Paris-Sud 11, CNRS/IN2P3, Orsay, France*
[7]*Institute of Nuclear Research, H-4001 Debrecen, Pf.51, Hungary*
[8]*FLNR, JINR, 141980 Dubna, Moscow region, Russia*
[9]*IPHC, CNRS/IN2P3 and Université de Strasbourg, F-67037 Stasbourg Cedex 2, France*

(Received 25 May 2010; published 1 September 2010)

The structure of ^{44}S has been studied by using delayed γ and electron spectroscopy. The decay rates of the 0_2^+ isomeric state to the 2_1^+ and 0_1^+ states, measured for the first time, lead to a reduced transition probability $B(E2\colon 2_1^+ \rightarrow 0_2^+) = 8.4(26)\ e^2\,\mathrm{fm}^4$ and a monopole strength $\rho^2(E0\colon 0_2^+ \rightarrow 0_1^+) = 8.7(7) \times 10^{-3}$. Comparisons to shell model calculations point towards prolate-spherical shape coexistence, and a two-level mixing model is used to extract a weak mixing between the two configurations.

DOI: 10.1103/PhysRevLett.105.102501 PACS numbers: 23.20.Lv, 25.70.Mn, 27.40.+z, 29.30.Kv

"Magic" nuclei exhibit large gaps between the occupied and valence orbits. They are cornerstones of the nuclear structure, being used (i) to test our understanding of the nuclear forces which form these gaps and (ii) to model more complicated systems having many valence nucleons. While nuclei having 8 and 20 protons (or neutrons) can be reproduced by modeling the atomic nucleus with an harmonic oscillator potential, a spin-orbit interaction must be added to describe heavier magic nuclei. This spin-orbit interaction strongly binds nucleons having their angular momenta ℓ aligned with their intrinsic spin value s, denoted as $\ell_\uparrow$. This leads throughout the chart of nuclei to a regular sequence of orbits $\ell_\uparrow$, $(\ell-2)_\uparrow$, $(\ell-2)_\downarrow$, $\ell_\downarrow$, with the so-called large spin-orbit gaps 14, 28, 50, 82, and 126 between the lowered $\ell_\uparrow$ orbit ($\ell = 2$, 3, 4, 5, and 6) and the others. Generally, in particular at the stability, these gaps are large enough to prevent excitations, and these magic nuclei are spherical. However, as the orbits forming the gap are separated by two units of angular momentum, quadrupole excitations are likely to develop if the shell gap is reduced. In this hypothesis, the development of quadrupole excitations jeopardizes the rigidity of the spherical gap and conduct the nucleus to deform. Consequently, the doubly magic nuclei which have proton and neutron spin-orbit shell closures could become vulnerable to quadrupole excitations, as both protons and neutrons could act coherently to deform the nucleus. So far, the prototypical deformed nucleus composed of such a double spin-orbit shell closure is $^{42}_{14}\mathrm{Si}_{28}$ [1]. At $N = 28$ a gradual development of deformation occurs between the spherical $^{48}_{20}\mathrm{Ca}_{28}$ and the deformed $^{42}_{14}\mathrm{Si}_{28}$. In between these two extremes, i.e., in $^{44}_{16}\mathrm{S}_{28}$, competition between spherical and deformed shapes is expected to be present, leading to shape coexistence [2–4]. Depending on the strength of the quadrupole correlations, either the spherical normal configuration or the deformed one becomes the ground state while the other configuration forms a low-lying 0_2^+ state. Therefore, the discovery and characterization of this 0_2^+ state in $^{44}\mathrm{S}_{28}$ represent crucial information for understanding the evolution of the $N = 28$ shell gap. The nonspherical nature of the ^{44}S ground state was suggested by its short β half-life and weak neutron-delayed emission probability [5], the low energy of the 2_1^+ state [1297(18) keV], and the enhanced reduced transition probability $B(E2\colon 2_1^+ \rightarrow 0_1^+)$ of 63(18) $e^2\,\mathrm{fm}^4$ [6]. However, the $E(2_1^+)$ and $B(E2)$ values are intermediate between a rigid rotor and a spherical nucleus. It suggests a possible mixing of spherical and deformed shapes which can be deduced by studying the properties of the 0_2^+ isomer at 1365(1) keV observed in Ref. [7]. Already the study of a $7/2^-$ isomer in ^{43}S [8,9] has shed light on shape coexistence in the $N \approx 28$ region. Other cases of shape coexistence around shell closures have been reported in Refs. [10,11].

The present Letter reports on the determination of the monopole strength $\rho^2(E0\colon 0_2^+ \rightarrow 0_1^+)$ and the reduced transition probability $B(E2\colon 2_1^+ \rightarrow 0_2^+)$ in ^{44}S, extracted from the measurement of the half-life and the branching ratio between the $E0$ and $E2$ decay of the isomeric 0_2^+ state. These pieces of information were obtained by using combined γ and electron-delayed spectroscopy and are used to demonstrate the shape coexistence in ^{44}S.

The experiment was carried out at the GANIL facility. A primary beam of ^{48}Ca at 60 $A \cdot$ MeV ($I \sim 2\ e\ \mu$A) impinged onto a 138 mg/cm^2 Be target to produce neutron-rich fragments separated by the LISE3 spectrometer [12] using an achromatic 100 mg/cm^2 Be degrader. The ^{44}S nuclei were produced at a rate of 200 sec^{-1} ($\Delta p/p = \pm 1.45\%$). Fragments were identified by means of their energy loss and magnetic rigidity ($B\rho$) values. The $B\rho$ was obtained from the position of the fragments at the dispersive focal plane given by a multiwire proportional chamber (CAVIAR) [13]. The selected nuclei were implanted in a 125 μm-thick kapton foil tilted at 20° with respect to the beam axis. Before the foil, a stack of Si detectors, including a XY position-sensitive one, was used to adjust the implantation depth and to reconstruct the position of the ions in a plane perpendicular to the beam axis. A thick Si detector located downstream from the implantation foil was used as a veto. Electrons were detected in four cooled 45×45 mm^2, 4 mm thick Si(Li) detectors, placed 20 mm above and below the beam axis. The γ rays were measured by two clover Ge detectors (EXOGAM) located on the side of the implantation foil, at a distance of 25 mm to the beam axis. The use of a parallel beam optics enables us to derive the ion implantation profile on the kapton foil from the XY Si detector. This ion profile, the geometry of the detectors, and that of the chamber were used as ingredients in a GEANT4 simulation to derive the electron (ϵ_{e^-}) and γ (ϵ_γ) efficiencies. The simulated efficiencies compare well with the ones obtained with calibrated sources of ^{207}Bi and ^{152}Eu placed in calibration runs at 6 different positions on the implantation foil. Using these comparisons, $\epsilon_\gamma = 3.06(5)\%$ and $\epsilon_{e^-} = 13.3(6)\%$ were adopted for a γ ray of 1329 keV and an electron of 1362.5 keV, respectively [14].

The decay of the 0_2^+ to the ground state ($E0$) proceeds through the emission of an internal conversion electron (IC) and by internal pair formation (IPF). The electron spectrum is shown in Fig. 1. A single peak is observed at 1362.5(10) keV corresponding to an excitation energy of 1365(1) keV for the 0_2^+ state, after having corrected for the binding energy of the K electrons. The integral of the peak is $I_{e^-_{\rm IC}}(E0) = 148(8) \times 10^3$. The low energy part of the spectrum is well accounted for by the IPF mechanism in which electrons and positrons share an energy of 343 keV. The fit of the electron time distribution (inset in Fig. 1) leads to a half-life of 2.619(26) μ sec , which agrees with the value of 2.3(5) μ sec reported in Ref. [7].

The $0_2^+ \rightarrow 2_1^+$ decay branch occurs through a strongly converted $E2$ transition at 36(1) keV, an energy below the experimental threshold of the detection system. The energy of this unobserved transition is derived from the measured energies of the 0_2^+ and 2_1^+ states, the latter being obtained from the observation of a delayed $2_1^+ \rightarrow 0_1^+$ transition at 1329.0(5) keV [half-life of 2.66(23) μ sec , in agreement with the value obtained from the electron spectrum] which follows the $0_2^+ \rightarrow 2_1^+$ decay. The 1329 keV energy agrees with the value of 1297(18) found in Ref. [6]. The yield of the $0_2^+ \rightarrow 2_1^+$ transition, $I_\gamma(E2)$, has been extracted from the number of delayed $2_1^+ \rightarrow 0_1^+$ γ rays. This transition is contaminated by the 1332.5 keV γ ray of ^{60}Co arising from the activation of the last selection slits of the spectrometer, which also produce in cascade a 1173 keV γ ray (inset in Fig. 2). The intensity of the 1329 keV peak has been obtained by a fit with two Gaussians, the intensity of the 1332.5 keV transition being constrained by that of the 1173 keV γ ray. The resulting $I_\gamma(E2)$ is $56(3) \times 10^3$.

The decay of the 0_2^+ state occurs through $E2$ and $E0$ transitions, the ratio of which is expressed as

$$R = \frac{\lambda(E2)}{\lambda(E0)} = \frac{I_\gamma(E2)}{I_{e^-_{\rm IC}}(E0)} \frac{1 + \alpha_{\rm conv}(2_1^+ \rightarrow 0_1^+)}{1 + \frac{\Omega_{\rm IPF}}{\Omega_{\rm IC}}}. \quad (1)$$

In this expression, the electronic factors for IPF and IC have been extrapolated for a nucleus with $A = 44$ from Refs. [15–17] to be $\Omega_{\rm IPF} = 1.495 \times 10^7$ sec^{-1} and

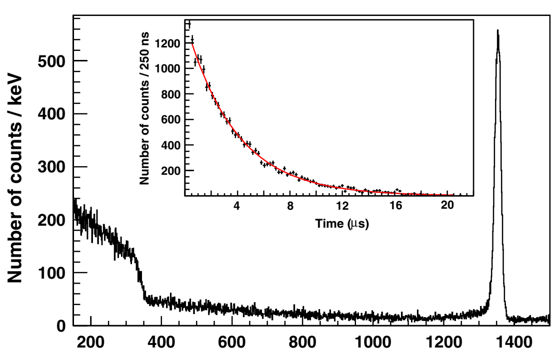

FIG. 1 (color online). Electron energy spectrum obtained from the Si(Li) detectors. The peak at 1362.5(10) keV corresponds to the $0_2^+ \rightarrow 0_1^+$ $E0$ transition. The low energy part is due to pair creation. Inset: Time distribution of the 1362.5 keV electron peak from which a half-life of 2.619(26) μ sec is extracted.

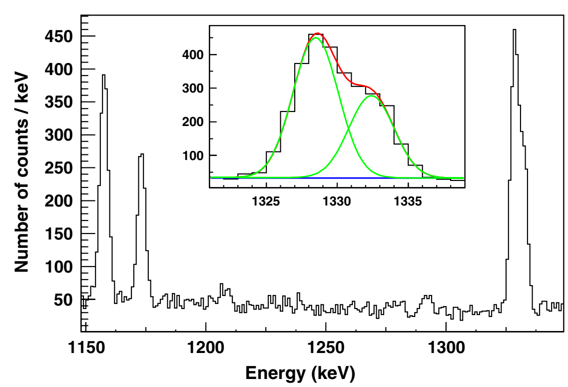

FIG. 2 (color online). Part of the delayed gamma energy spectrum. Peaks from the β decay of ^{44}K (1158 keV) and ^{60}Co (1173 and 1332.5 keV) are identified, the latter overlapping with the 1329 keV $2_1^+ \rightarrow 0_1^+$ transition of ^{44}S. The deconvolution of this doublet is shown in the inset.

TABLE I. Experimental and shell model values for the excitation energies, in MeV, and reduced transition probabilities $B(E2)$, in $e^2\,\mathrm{fm}^4$, of ^{44}S.

$E/B(E2)$	2_1^+	0_2^+	2_2^+	$2_1^+ \to 0_1^+$	$2_1^+ \to 0_2^+$
Exp.	1.329(1)	1.365(1)	2.335(39)	63(18)	8.4(26)
SM	1.172	1.137	2.140	75	19

$\Omega_{\mathrm{IC}} = 1.1125 \times 10^7\ \mathrm{sec}^{-1}$, respectively. A value of 3.6×10^{-5} has been taken for the conversion coefficient $\alpha_{\mathrm{conv}}(2_1^+ \to 0_1^+)$ [18]. By using the experimental values of $I_{e^-_{\mathrm{IC}}}(E0)$ and $I_\gamma(E2)$ derived above, the resulting branching ratio is $R = 0.163(13)$. The $\rho^2(E0\text{: } 0_2^+ \to 0_1^+)$ and $B(E2\text{: } 2_1^+ \to 0_2^+)$ values are obtained by using the following equations:

$$\rho^2(E0) = \frac{\ln(2)}{T_{1/2}(0_2^+)(1 + R)(\Omega_{\mathrm{IPF}} + \Omega_{\mathrm{IC}})}, \qquad (2)$$

$$B(E2) = \frac{5.65 \times 10^{-10}}{5E_\gamma^5 T_{1/2}(1 + \frac{1}{R})[1 + \alpha_{\mathrm{conv}}(0_2^+ \to 2_1^+)]}. \qquad (3)$$

By using the measured branching ratio R, the half-life value $T_{1/2}(0_2^+)$, and $\alpha_{\mathrm{conv}}(0_2^+ \to 2_1^+) = 10.94(1)$ extrapolated from Ref. [18], the monopole strength $\rho^2(E0\text{: } 0_2^+ \to 0_1^+)$ and the reduced transition probability $B(E2\text{: } 2_1^+ \to 0_2^+)$ have been determined to be $8.7(7) \times 10^{-3}$ and $8.4(26)\ e^2\,\mathrm{fm}^4$, respectively.

The values of $E(0_2^+) = 1365(1)$ keV and $\rho^2(E0) = 8.7(7) \times 10^{-3}$ are the smallest measured in this mass region, pointing to a weak mixing between the 0_1^+ ground state and the 0_2^+ isomer and therefore to shape coexistence. In the case of a large mixing, these states would repel each other to exhibit a large energy spacing and a larger $\rho^2(E0)$ value. To obtain further understanding on the nature of the shape coexistence, data are compared to shell model calculations.

Shell model (SM) calculations have been performed for $^{44}_{16}\mathrm{S}_{28}$ by using the ANTOINE code [19] and the SDPF-U interaction that accounts remarkably well for the nuclear structure in this region [20]. The full sd (fp) valence space has been used for protons (neutrons) with standard effective charges $e_\pi = 1.35e$ $(e_\nu = 0.35e)$. The results gathered in Table I show good agreement with the experimental values; the only exception is a somewhat larger calculated $B(E2\text{: } 2_1^+ \to 0_2^+)$ value than measured. Nevertheless, both experiment and calculation agree with the fact that the 2_1^+ state connects much strongly with the 0_1^+ state than with the 0_2^+ one. Indeed, the experimental $B(E2\text{: } 2_1^+ \to 0_1^+)/B(E2\text{: } 2_1^+ \to 0_2^+)$ ratio is 7.5, whereas the calculated one is 3.2. Calculated excited states connected to these two 0^+ states are presented in Fig. 3 with their intrinsic quadrupole moments Q_0. For the sake of clarity, only the states of present interest are shown in this picture. Remarkable is the presence of 2_1^+, 4_2^+, and 6_2^+ states on top of the 0_1^+ ground state connected by large $B(E2)$ values and having equal Q_0 values of about 60 $e\,\mathrm{fm}^2$. These two features characterize a rotational band of an axially deformed nucleus with $\beta \simeq 0.25$. The 2_2^+ state at 2.14 MeV has a smaller $Q_0 = -0.3\ e\,\mathrm{fm}^2$ compatible with a spherical shape. A candidate for the 2_2^+ state is proposed at 2335(39) keV by placing the previously reported 988 keV transition [21] on top of the 0_2^+ or 2_1^+ state. Hence, SM calculations suggest a prolate-spherical shape coexistence in ^{44}S.

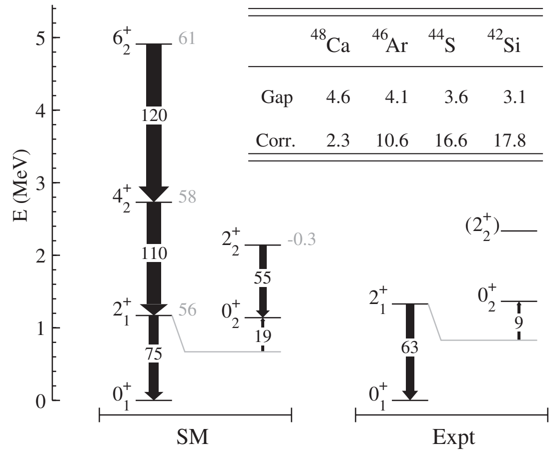

FIG. 3. ^{44}S level scheme calculated within the present SM approach (left) compared with available experimental data (right). $E2$ transition probabilities (in $e^2\,\mathrm{fm}^4$) are reported on top of black arrows, and intrinsic quadrupole moments (in $e\,\mathrm{fm}^2$) are shown in light gray on the right side of calculated levels. The ground state of the nucleus is head of a rotational band ($\beta \simeq 0.25$) and coexists with the rather spherical low-lying 0_2^+ isomer. Calculated values of the $N = 28$ gap and correlation energies (in MeV) are given for even-even $N = 28$ isotones.

A detailed analysis of the components contributing to the total energy of the 0^+ states has been performed in order to deepen our understanding of the evolution of the collectivity from $^{48}_{20}$Ca to $^{42}_{14}$Si. Within the SM framework, the total Hamiltonian can be separated into its monopole (i.e., spherical mean-field contribution) and multipole (i.e., correlations mainly of pairing and quadrupole type) parts [22]. As can be seen from the values reported in Fig. 3, correlations strongly increase from the doubly magic ^{48}Ca ($\simeq 2$ MeV) down to the ^{42}Si ($\simeq 18$ MeV), while the size of the $N = 28$ shell gap gets slightly reduced [23]. This increase of correlations is favored, on one hand, by neutron quadrupole excitations across the $N = 28$ gap between the $f_{7/2}$ and $p_{3/2}$ orbits [23] and, on the other hand, by the degeneracy of proton $s_{1/2}$ and $d_{3/2}$ orbits and excitations from the $d_{5/2}$ shell [1,24–26]. In both cases, quadrupole correlations are favored by the fact that occupied and valence states are separated by two units of angular momentum. Without considering multipole contributions to the 0_1^+ and 0_2^+ states in ^{44}S, both levels are found to be quasidegenerate in energy, and the ground state of ^{44}S is spherical. A gain of 1.5 MeV from the multipole energy brings the deformed configuration at the minimum of binding energy, while the spherical configuration corresponds to the excited state. Similar multipole effects energetically favor the oblate 0^+ state in ^{42}Si which is predicted to coexist with a prolate 0^+ state [20] at 1293 keV.

The SM calculation uses an harmonic oscillator basis for the description of the atomic nucleus and the calculated $E0$ transition between states of the same harmonic oscillator shells, as for protons in the sd shells and neutron in the fp shells, is strictly zero. Therefore, in order to shed light on the amount of mixing between the $0^+_{1,2}$ states and to deduce their shape before mixing, we use a phenomenological two interacting levels model. We assume two spherical (S) and deformed (D) states before mixing which interact to produce 0^+_1 and 0^+_2 states defined as $|0_1\rangle = \cos\theta|0_D\rangle + \sin\theta|0_S\rangle$ and $|0_2\rangle = -\sin\theta|0_D\rangle + \cos\theta|0_S\rangle$, where θ is the mixing angle. The $E2$ transition between the 2^+_1 and 0^+_2 (or 0^+_1) states being mainly due to the D component of these 0^+ states, it follows that $B(E2{:}\ 2^+_1 \rightarrow 0^+_2)/B(E2{:}\ 2^+_1 \rightarrow 0^+_1) \sim \tan^2(\theta)$ [Eq. (2) of [27]]. A mixing amplitude $\tan^2(\theta) = 0.13$ is deduced from the experimental $B(E2)$ values, whereas the shell model gives a somewhat larger value of 0.24, both being smaller than the case of a maximum mixing $[\tan^2(\theta) = 1]$. Therefore, the shape coexistence is found to be more pronounced experimentally than calculated by the SM. The magnitude of the monopole matrix element can be written as a function of the mixing amplitude and of the difference of shapes β_S and β_D before mixing [28]: $\rho^2(E0) = (3Ze/4\pi)^2\sin^2\theta\cos^2\theta(\beta_D^2 - \beta_S^2)^2$. By using the experimental value of $\tan^2(\theta)$, the experimental ρ^2 is reproduced only when $\beta_D \simeq 0.274$ and $\beta_S = 0$ are assumed. The deformation parameter β_D is in close agreement with the values obtained after mixing from Coulomb excitation experiment [6], $\beta = 0.258(36)$, and from the SM calculations, $\beta = 0.25$. Altogether these values again point towards a deformed-spherical shape coexistence in ^{44}S.

In summary, electron and γ delayed spectroscopy has been used to determine the monopole strength $\rho^2(E0{:}\ 0^+_2 \rightarrow 0^+_1) = 8.7(7) \times 10^{-3}$ and the reduced transition probability $B(E2{:}\ 2^+_1 \rightarrow 0^+_2) = 8.4(26)\ e^2\,\mathrm{fm}^4$ in the $^{44}_{16}S_{28}$ nucleus. By using these values, the earlier measured $B(E2{:}\ 2^+_1 \rightarrow 0^+_1)$ [6], shell model calculations, and a two-level mixing model, it is found that ^{44}S exhibit a shape coexistence between a prolate ground state ($\beta \simeq 0.25$) and a rather spherical 0^+_2 state. This establishes how the onset of collectivity progressively develops between the spherical $^{48}_{20}Ca$ and the deformed $^{42}_{14}Si$ nuclei. This study completes uniquely the understanding of the shell-breaking mechanism at the spin-orbit closed-shell $N = 28$, which is as well of importance for the evolution of other shell gaps having the same origin.

We are grateful to the GANIL staff and the LISE team for support. We acknowledge P. Van Isaker for fruitful discussions. This work was supported by CNCSIS-UEFISCSU, Project No. PNII-IDEI 933/2007, Academy of Sciences of Czech Republic, and by the European Community through OTKA K68801.

[1] B. Bastin *et al.*, Phys. Rev. Lett. **99**, 022503 (2007).
[2] T.R. Werner *et al.*, Nucl. Phys. **A597**, 327 (1996); P.-G. Reinhard *et al.*, Phys. Rev. C **60**, 014316 (1999); G.A. Lalazissis *et al.*, Phys. Rev. C **60**, 014310 (1999); R. Rodriguez-Guzman, J.L. Egido, and L.M. Robledo, Phys. Rev. C **65**, 024304 (2002).
[3] S. Péru, M. Girod, and J.F. Berger, Eur. Phys. J. A **9**, 35 (2000).
[4] E. Caurier, F. Nowacki and A. Poves, Nucl. Phys. **A742**, 14 (2004).
[5] O. Sorlin *et al.*, Phys. Rev. C **47**, 2941 (1993).
[6] T. Glasmacher *et al.*, Phys. Lett. B **395**, 163 (1997).
[7] S. Grévy *et al.*, Eur. Phys. J. A **25**, 111 (2005).
[8] F. Sarazin *et al.*, Phys. Rev. Lett. **84**, 5062 (2000).
[9] L. Gaudefroy *et al.*, Phys. Rev. Lett. **102**, 092501 (2009).
[10] S. Shimoura *et al.*, Phys. Lett. B **560**, 31 (2003); **654**, 87 (2007).
[11] W. Schwerdtfeger *et al.*, Phys. Rev. Lett. **103**, 012501 (2009).
[12] R. Anne *et al.*, Nucl. Instrum. Methods Phys. Res., Sect. A **257**, 215 (1987).
[13] L. Perrot *et al.*, in Proceedings of the 11th International Conference on Heavy Ion Accelerator Technology, Venice, Italy, 2009 (unpublished), http://cern.ch/AccelConf/HIAT2009/papers/g-02.pdf.
[14] http://tel.archives-ouvertes.fr/docs/00/43/01/25/PDF/Manuscrit_These_final.pdf.
[15] A. Passoja and T. Salonen, JYFL Report No. JYFL RR-2/86, 1986 (unpublished).
[16] E.L. Church and J. Weneser, Phys. Rev. **103**, 1035 (1956).
[17] D.H. Wilkinson *et al.*, Nucl. Phys. **A133** 1 (1969).
[18] I.M. Band *et al.*, At. Data Nucl. Data Tables **18**, 433 (1976).
[19] E. Caurier *et al.*, Rev. Mod. Phys. **77**, 427 (2005).
[20] F. Nowacki and A. Poves, Phys. Rev. C **79**, 014310 (2009).
[21] D. Sohler *et al.*, Phys. Rev. C **66**, 054302 (2002).
[22] M. Dufour and A.P. Zuker, Phys. Rev. C **54**, 1641 (1996).
[23] L. Gaudefroy *et al.*, Phys. Rev. Lett. **99**, 099202 (2007).
[24] L.A. Riley *et al.*, Phys. Rev. C **78**, 011303 (2008).
[25] L. Gaudefroy, Phys. Rev. C **81**, 064329 (2010).
[26] M. De Rydt *et al.*, Phys. Rev. C **81**, 034308 (2010).
[27] H. Mach *et al.*, Phys. Lett. B **230**, 21 (1989).
[28] J.L. Wood *et al.*, Nucl. Phys. **A651**, 323 (1999).